AIAA JOURNAL
Vol. 42, No. 8, August 2004

Unsteady Reynolds-Averaged Navier–Stokes Computations of Transitional Wake/Blade Interaction

S. Lardeau* and M. A. Leschziner†
Imperial College London, London, England SW7 2AZ, United Kingdom

The interaction between wakes generated by a moving array of cylindrical bars and the transitional boundary layer over a low-pressure turbine blade located downstream of the bars is studied by means of an unsteady Reynolds-averaged Navier–Stokes (RANS) method that incorporates a recent low-Reynolds-number, nonlinear eddy-viscosity turbulence model. The context of the study is the modelling of unsteady rotor/stator-interaction phenomena. A number of issues pertaining to the ability of the unsteady RANS approach to simulate this interaction within a phase-averaged framework are investigated, including numerical accuracy and resolution, the consequence of vortex shedding from the bars, the characteristics of the wake within the blade passage, and the ability of the model to return the transitional response of the boundary layer to the dynamics of and the turbulence transported by the wakes. The results of an initial investigation, in which both the moving bars and the blade are included in the computation, show this approach to be ill-suited to a phase-averaged framework. As an alternative, the wake conditions just behind the bar are extracted from a precursor simulation in which the wake is subjected to averaging before being prescribed, and this approach is shown to be both appropriate and effective. The evolution of the wake in the blade passage is well predicted with this method. Moreover, the unsteady wake-induced transition process is also well reproduced in comparison with experiment, but there are indications that the relative roles of the (essentially inviscid) wake dynamics and the turbulence within the wake in effecting transition and relaminarization in the boundary layer differ somewhat from those gleaned from the experiment.

Nomenclature

a_{ij}	=	anisotropy tensor
C	=	blade-chord length
D	=	diameter of the bar
f_ω	=	wall-damping function
H	=	shape factor, δ_1/δ_2
k	=	turbulence energy
n^*	=	nondimensional wall distance, $u_\varepsilon n/\nu$
R_t	=	turbulent Reynolds number, $k^2/\nu\varepsilon$
S_{ij}	=	strain tensor
s	=	coordinate along the suction side of the blade
T	=	period for one passage of the bar
Tu	=	turbulence intensity
U_b	=	streamwise velocity of the incoming flow
$\overline{u_i u_j}$	=	Reynolds stress tensor
u_ε	=	Kolmogorov velocity scale, $(\nu\varepsilon)^{1/4}$
V_x	=	vertical velocity of the moving bar
δ_1	=	displacement thickness
δ_2	=	momentum thickness
ε	=	dissipation rate of turbulence energy
ν	=	viscosity
ν_t	=	turbulent viscosity
Ω_{ij}	=	vorticity tensor
ω	=	specific dissipation rate, ε/k

I. Introduction

WAKE/BLADE interaction is an inherent feature of turbomachine aerodynamics and the principal cause of unsteadiness in the flow around blades. The interaction has a number of facets, some inviscid and others viscous. The focus of this paper is on the latter aspects, in the context of the performance of low-pressure-stage turbine blades.

The wake generated by a blade contains a mean-velocity defect and turbulence, both of which arise from a combination of processes in the boundary layers developing on the blade's surface and from separation behind the, usually, rounded trailing edge. The latter phenomenon is itself unsteady, due to alternate shedding of vortices from the suction and pressure sides. Thus, the wake contains stochastic turbulence, as well as periodic vortices, that decay relatively quickly due to spanwise break up.

When a wake enters the blade passage of a downstream stage, the momentum defect provokes unsteady distortions and transverse motions within the passage flow, with consequent unsteady perturbations in the boundary layers. At least as important as this largely inviscid interaction is the effect of the turbulence transported with the wake on the transitional suction-side boundary layer.

The response of the boundary layer to wake turbulence is of particular interest in low-pressure (LP) turbine stages. The relatively low operational Reynolds numbers of these stages and the strong favourable pressure gradient along the blade passages result in a significant proportion of the boundary layers on both suction and pressure sides remaining laminar. Toward the trailing edge, however, the suction-side boundary layer may be subjected to a locally adverse pressure gradient, and this can easily provoke laminar separation. In such circumstances, it is desirable to induce transition on the suction side to avoid separation, and this is precisely what is achieved with the wakes.

The physical processes contributing to wake-induced transition are complex and poorly understood. Transition is known to be affected by numerous issues, among them free-stream turbulence, pressure gradient, curvature, surface roughness, and inertial perturbations, both upstream of the boundary layer and in the freestream above it. Light on the fundamental interactions at play is being shed, for some simple conditions, principally by direct and large eddy simulations.[1–3] These show that wake-induced transition is, essentially, a top-down process in which turbulent spots are generated in the upper part of the boundary layer and then propagate downward. A feature observed repeatedly, both in simulations and experiments,[4–8] is that, especially at low freestream turbulence, wake-induced transition is followed by relaminarization (calming)

Received 15 August 2003; revision received 3 March 2004; accepted for publication 19 March 2004.

*Research Associate, Department of Aeronautics, Prince Consort Road, South Kensington.

†Professor, Department of Aeronautics, Prince Consort Road, South Kensington.

and then by retransition close to the trailing edge. Hence, transition is highly intermittent and only sustained in the presence or proximity of the wake and its turbulence cloud.

The prediction of the preceding interactions with statistical closures is a major challenge. Numerous studies on steady transition in flow over flat plates at different combinations of freestream turbulence intensities and pressure gradients[7] demonstrate the frailties of turbulence models, whether applied in their classical form[8] or in combination with transition-specific models, the latter usually based on the concept of intermittency parameterisation.[9,10] Very few models give a consistent performance over even a modest range of conditions. Recent efforts[11] have focused on combining low-Reynolds-number nonlinear eddy-viscosity models with intermittency-based approaches, not only in an effort to improve the prediction of the transition itself, but also to return the buildup of turbulence (or unsteady fluctuations) in the boundary layer well ahead of the sudden rise in skin friction, observed both experimentally and in simulations. In the present context, the use of a low-Reynolds-number turbulence model is imperative, because the flow undergoes repeated transition, relaminarization, and retransition, events that are intimately linked to viscous damping of turbulence.

In unsteady conditions, a general problem with statistical approaches lies in the fundamental conflict between the concept of Reynolds-averaging and the unsteadiness. Associated with this is the problem that virtually all available turbulence closures have been formulated and calibrated by reference to steady flows, in which turbulence is close to a state of equilibrium. Thus, the concept of unsteady Reynolds-averaged Navier–Stokes (URANS) is, in itself, subject to uncertainties, unless there is a clear separation between the turbulence scales and that associated with the unsteadiness. Even if such a separation applies to the unsteadiness associated with the motion of the wake as a whole, this will not pertain to the shedding behind the blade, which is characterized by a much shorter timescale than that of the wake. When, as is the case herein, the focus is on a spanwise homogeneous flow, so that a two-dimensional RANS procedure can be applied with major rewards in economy,[12–14] vortex shedding causes the additional serious problem of a grossly excessive level of periodicity and coherence in the wake because of the absence of a mechanism for spanwise vortex breakup. It is observed, therefore, as will be demonstrated later, that the statistical representation derived from two-dimensional URANS in the far wake ($x/D > 6$) of a circular cylinder is poor when compared to a full three-dimensional simulation. Correspondingly, when a wake/blade-interaction computation includes the obstacle that generates the wakes (the upstream blade or an equivalent bluff body), the wake entering the passage, unless averaged, is contaminated by the much too vigorous periodic component associated with the shedding. This then leads to a misrepresentation of the wake/blade-interaction processes.

The flow considered herein consists of a plane cascade of LP blades and an upstream array of circular rods, the latter generating the wakes, moving relative to the cascade, and representing the effect of upstream rotor blades. The configuration was examined experimentally by Stieger.[15] The moving circular cylinders have been chosen such that the wakes have similar properties, in terms of velocity deficit and turbulent kinetic energy in the wake, to those behind the rotor blade. Although strong vortex shedding occurs behind the cylinders, the phase-averaged measurements, with reference to the pitchwise period, do not feature the unsteadiness associated with shedding. Correspondingly, the URANS computations regard the flow in phase-averaged terms and should not feature vortex shedding either. However, the inclusion of the moving rods in the computation necessarily results in the shedding being resolved (provided that the computational grid and the time step are sufficiently fine). Hence, as will be shown, the approach that must be adopted here is to prescribe the moving, phase-averaged wake at the upstream boundary of the computational domain. The need for such a practice has serious implications to any RANS approach used in practice to resolve wake/blade interaction.

The aforementioned methodology of the use of an averaged representation of the wake at the inlet has also been adopted by Wu and Durbin[16] and Michelassi et al.[2] in their direct numerical and large eddy simulations, respectively. However, this was done for reasons entirely different from those relating to the present URANS computations. In a simulation, there is, fundamentally, a good reason to include the moving upstream rod (or blade) and to perform the requisite number of pitchwise traverses to determine the phase-averaged state. However, this would be an extremely costly approach. Moreover, as shedding-associated periodicity decays quickly, in reality,[17] the treatment adopted in the simulations can be defended if the wake is generated sufficiently far from the downstream blade passage.

The aim of this paper is to highlight the challenges, both numerical and physical, that have to be met in URANS computations of wake/blade interaction. As in any URANS application, the solution has to be converged, both in terms of the grid and time step. In the first part of the paper, this requirement will be shown to give rise to serious resource-related implications in the present circumstances. Several important issues, including numerical accuracy and the realism of the introduction of the wake, are addressed. Results of a wake/blade interaction, corresponding to the experiments of Stieger,[15] will then be presented. These results have been obtained by the use of what is considered to be the best possible approach to prescribing the wake.

II. Turbulence Models and Numerical Methods

The choice of a turbulence model for any application is far from a straightforward exercise. Here, the low-Reynolds-number, nonlinear eddy-viscosity model (strictly, an explicit algebraic Reynolds-stress model), proposed by Abe et al.,[18] has been adopted. This formulation offers a number of potential advantages. It is well-known that any one Reynolds stress is, in general, linked nonlinearly to all other stresses and strains and that such a linkage is established by nonlinear models. In the near-wall region, the normal-stress anisotropy is especially high, and the present model was especially calibrated to return the correct level of near-wall anisotropy, especially the asymptotic approach toward two-component wall turbulence. Another pertinent aspect in the context of the flow over a blade is that this model gives very good results for flow separating from curved surfaces.[19] Two principal versions of this model exist, one involving a length-scale-related equation for the dissipation rate ε and the other an equation for the specific dissipation $\omega = \varepsilon/k$. The former performs better for transitional flow[11] and has, therefore, been preferred in this study.

The ε-version of the model adopts a four-part representation of the effects of strain, vorticity, and wall-proximity on the anisotropy tensor:

$$a_{ij} = (\overline{u_i u_j}/k) - (2/3)\delta_{ij} = (2/C_D)\left\{c^*_{ij} + [1 - f_w(26)]\left(d^*_{ij} + e^*_{ij}\right) + C_D f_w(26) f^*_{ij}\right\} \quad (1)$$

in which c^*_{ij} relates linearly to the strain tensor, d^*_{ij} includes quadratic terms in the strain and vorticity tensors, e^*_{ij} is a term accounting specifically for strong normal straining, and f^*_{ij} relates to wall proximity and orientation. The last term is an especially important fragment, in so far as it is instrumental in securing the correct wall-asymptotic behavior of the anisotropy. In Eq. (1), f_w is the wall-related damping function

$$f_w(A) = \exp[-(n^*/A)^2] \quad (2)$$

where $n^* = u_\varepsilon n/\nu$ is the nondimensional wall distance and $u_\varepsilon = (\nu\varepsilon)^{1/4}$ is the Kolmogorov velocity scale.

The terms appearing in Eq. (1) are as follows:

$$c^*_{ij} = -C_B S^*_{ij}$$

$$d^*_{ij} = C_B\left[-2\left(S^*_{ik}\Omega^*_{kj} - \Omega^*_{ik}S^*_{kj}\right) + 2\left(S^*_{ik}S^*_{kj} - \frac{\delta_{ij}}{3}S^{*2}\right)\right]$$

$$e^*_{ij} = -C_B f_{s_1} S^*_{ij} + 2C_B f_{s_2}\left(S^*_{ik}S^*_{kj} - \frac{\delta_{ij}}{3}S^{*2}\right) \quad (3)$$

$$f_{ij}^{*} = -\alpha_\omega \frac{1}{2}\left(d_i d_j - \frac{\delta_{ij}}{3}\right) + \left(1 - fr_1^2\right)\left[\frac{-\beta_\omega C_\omega}{1 + C_\omega\sqrt{S^{**^2}\Omega^{**^2}}}\left(S_{ik}^{**}\Omega_{kj}^{**} - \Omega_{ik}^{**}S_{kj}^{**}\right) + \frac{\gamma_\omega C_\omega}{1 + C_\omega S^{**^2}}\left(S_{ik}^{**}S_{kj}^{**} - \frac{\delta_{ij}}{3}S^{**^2}\right)\right]$$

$$C_B = \frac{1}{1 + (22/3)\Omega^{*2} + (2/3)\left[\Omega^{*2} - S^{*2}\right][1 + 100(\Omega^{*} - S^{*})]}$$

where

$$S_{ij}^{*} = C_D\tau S_{ij}, \qquad \Omega_{ij}^{*} = C_D\tau\Omega_{ij}, \qquad S_{ij}^{**} = \tau_d S_{ij}$$

$$\Omega_{ij}^{**} = \tau_d\Omega_{ij}, \qquad C_D = 0.8 \tag{4}$$

$$S^{*^2} = S_{mn}^{*}S_{mn}^{*}, \qquad \Omega^{*^2} = \Omega_{mn}^{*}\Omega_{mn}^{*}$$

$$S^{**^2} = S_{mn}^{**}S_{mn}^{**}, \qquad \Omega^{**^2} = \Omega_{mn}^{**}\Omega_{mn}^{**} \tag{5}$$

$$S^{*} = \sqrt{S^{*^2}}, \qquad \Omega^{*} = \sqrt{\Omega^{*^2}}$$

$$f_{s_1} = f_{r_1}f_{r_2}15\left(\Omega^{*^2} - S^{*^2}\right), \qquad f_{s_2} = -f_{r_1}f_{r_2}\left[1 + 7\left(\Omega^{*^2} - S^{*^2}\right)\right] \tag{6}$$

$$f_{r_1} = \frac{\Omega^{*^2} - S^{*^2}}{\Omega^{*^2} + S^{*^2}}, \qquad f_{r_2} = \frac{S^{*^2}}{\Omega^{*^2} + S^{*^2}} \tag{7}$$

Two different sets of coefficients are given by Abe et al.[18]

Model 1:

$$\alpha_\omega = 1, \qquad \beta_\omega = \tfrac{1}{4}, \qquad \gamma_\omega = 1.5, \qquad C_\omega = 0.5 \tag{8}$$

Model 2:

$$\alpha_\omega = 0, \qquad \beta_\omega = 5/12, \qquad \gamma_\omega = 0.5, \quad C_\omega = 1 \tag{9}$$

Unless stated otherwise, model 1 [Eq. (8)] is used in the following considerations. The term d_i represents the wall-normal direction. In the work of Abe et al.,[18] this term is based on the wall distance n, and it takes the form

$$d_i = \frac{N_i}{\sqrt{N_k N_k}}, \qquad N_i = \frac{\partial n}{\partial x_i} \tag{10}$$

Finally, the timescale τ_d combines the turbulent macro scale and the Kolmogorov scale:

$$\tau_d = [1 - f_\omega(15)](k/\varepsilon) + f_\omega(15)\sqrt{\nu/\varepsilon} \tag{11}$$

In this formulation, use is made of the turbulence energy k and the dissipation rate ε to achieve the requisite dimensional consistency in Eq. (1). These scales are also needed to evaluate the turbulent viscosity,

$$\nu_t = c_\mu f_\mu(k^2/\varepsilon) \tag{12}$$

from which the timescale $\tau = \nu_t/k$ is obtained. The damping function

$$f_\mu = \left\{1 + \left(35\Big/R_t^{\frac{3}{4}}\right)\exp\left[-\left(R_t\Big/30\right)^{\frac{3}{4}}\right]\right\}[1 - f_w(26)] \tag{13}$$

represents the influence of fluid viscosity on its turbulent counterpart. The turbulence energy and its dissipation are derived, respectively, from

$$\frac{Dk}{Dt} = \frac{\partial}{\partial x_j}\left[\left(\nu + \frac{\nu_t}{\sigma_k}\right)\frac{\partial k}{\partial x_j}\right] - \underbrace{\overline{u_i u_j}\frac{\partial U_i}{\partial x_j}}_{P_k} - \varepsilon \tag{14}$$

$$\frac{D\varepsilon}{Dt} = \frac{\partial}{\partial x_j}\left[\left(\nu + \frac{\nu_t}{\sigma_\varepsilon}\right)\frac{\partial \varepsilon}{\partial x_j}\right] - c_{\varepsilon_1}\frac{\varepsilon}{k}\overline{u_i u_j}\frac{\partial U_i}{\partial x_j} - c_{\varepsilon_2}f_\varepsilon\frac{\varepsilon^2}{k} \tag{15}$$

where

$$\sigma_k = 1.2/f_t, \qquad f_t = 1 + 5.0 f_w(5) \tag{16}$$

$$f_\varepsilon = \left\{1 - 0.3\exp\left[-(R_t/6.5)^2\right]\right\}[1 - f_w(3.7)]$$

$$c_\mu = 0.12, \qquad c_{\varepsilon_1} = 1.45, \qquad c_{\varepsilon_2} = 1.83, \qquad \sigma_\varepsilon = 1.5/f_t \tag{17}$$

In a study of bypass transition in steady flow over a flat plate for a range of free-stream-turbulence levels and pressure-gradient fields, Lardeau et al.[11] show that the performance of the model by Abe et al.[18] can be substantially enhanced by the introduction of corrections relating to intermittency into it. However, here the model is used without these corrections, for two reasons. First, the corrections are based on observations in steady conditions in which the flow undergoes a single transition process that is dictated, within the model, by a delicate balance between the amplification of turbulence through a combination of diffusion and production and its attenuation by viscous effects. Whereas this balance may also be of relevance to the present unsteady environment, it is observed, experimentally, that transition is induced, at least for relatively low freestream turbulence, once the wake-turbulence cloud being convected through the passage reaches the boundary layer. Hence, the onset of transition appears to depend, primarily, on the ability of the simulation to represent the wake-turbulence transport faithfully through the passage and toward the boundary layer.[15] Second, experimental observations[6,20] suggest further that the behavior of the flow subsequent to transition depends on the response of the boundary layer to the removal of the wake turbulence from the edge of the boundary layer as the wake passes out of the passage. This response is not an issue addressed by the corrections introduced by Lardeau et al.[11]

The calculations reported hereafter have been performed with a multiblock version of the nonorthogonal, fully collocated, finite volume scheme STREAM by Lien et al.[21] This original version has been extended by Chen and Leschziner[22] to accommodate relative bar-blade movement by way of a sliding-mesh methodology. Convection of all transported properties is approximated by the use of the UMIST-TVD scheme,[23] and time marching is performed with a second-order scheme. The SIMPLE pressure-correction algorithm is used to enforce mass conservation within any one time step by means of in-step iteration.

III. Flow Configuration

The computed geometry is shown in Fig. 1 and consists of a single LP turbine blade, designated T106, enclosed within a pitchwise periodic segment that extends from one passage midsection to the next. This blade is subjected to wakes shed from moving bars located $0.35C$ upstream of the leading edge of the blade. The main geometric and flow parameters are listed in Table 1. Note that the freestream-turbulence intensity is unusually low for a practical turbine blade. This was held to be a potential problem in respect of turbulence modeling, because the representation of bypass

Table 1 Parameters for the T106A cascade

Parameter	Value
Chord length C	198 mm
Axial chord length	$0.8585C$
Reynolds number Re_C	0.97×10^5
Blade pitch	$0.798C$
Distance bar to leading edge	$0.35C$
Bar pitch	$0.798C$
Bar diameter	$0.01C$
Flow coefficient V_x/U_b	0.83
Freestream turbulence intensity Tu	1%

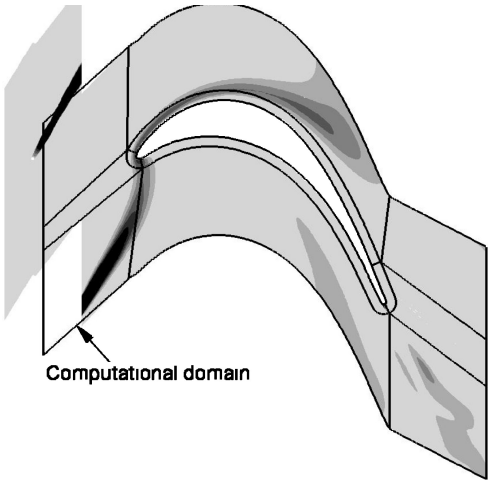

Fig. 1 Computational domain for the T106A test case.

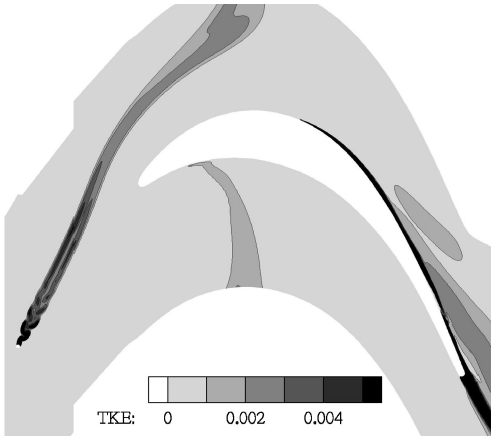

Fig. 2a Visualization of turbulence-energy k computed from the turbulence model within a full bar/blade computation (151,000 grid cells, 800 time steps per pitchwise traverse).

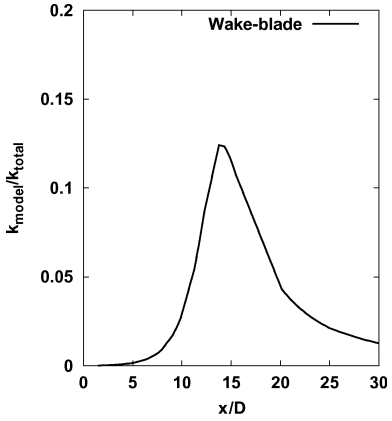

Fig. 2b Streamwise evolution of the ratio $k_{\text{model}}/k_{\text{total}}$ along the wake centerline.

transition by way of RANS models relies on diffusion of turbulence from the freestream into the laminar boundary layer.

As discussed in the Introduction, the inclusion of the bar within the framework of a phase-averaged representation of turbulence effects in a two-dimensional URANS computation is not promising. Figure 2 shows an instantaneous view of the wake when both bar and blade are included, by the use of the methodology of Chen and Leschziner.[22] In this computation, the time step and grid are sufficiently fine to allow the resolution of the shedding behind the cylindrical bar, as should be the case. Figures 2a and 2b show the high level of unsteadiness in the wake, associated with shedding, and gives the distribution, along the wake centerline, of the ratio of the modeled turbulence energy to the total of modeled and resolved components, the latter obtained from the time-integral of the unsteady kinetic energy. As seen, the resolved component strongly dominates over the modeled one.

A total of 151,000 cells are used within 12 blocks to describe the full passage shown in Fig. 1 (without the bar). This cell number might appear to be inordinately high for a two-dimensional flow, with frightening implications for three-dimensional computations, but it is necessary to avoid a significant level of numerical error in this type of flow in which a principal computational challenge is to convect time-changing scalar turbulence quantities across a highly skewed grid. (See Lardeau and Leschziner[24] for a detailed study of the numerical accuracy for this type of configuration.) The inflow conditions were prescribed at $0.32C$ upstream of the blade's leading edge, the choice of this particular location to be justified later. To this end, a method was required to generate the wake at the inflow plane. One possibility explored was to use experimental data. However, such data were not available at a distance upstream of the blade at which potential effects were insignificant. Moreover, the data were not sufficiently resolved and also only applied to one specific configuration. Here, a computational route was, therefore, taken.

First, a precursor simulation was performed for the full bar/blade domain (Fig. 2), with the block associated with the bar moved relative to the cascade at the correct speed and with the correct conditions prescribed well upstream of the bar. For this precursor simulation, a fine grid of 141,000 cells and 800 time steps per pitchwise traverse were used. Test calculations[24] had shown these conditions to result in a grid- and time-step independent solution for the bar wake. The time-average state of the wake along the plane $x = -0.32C$, at which the wake was to be prescribed in the final calculation, was then computed in a moving frame of reference attached to the bar.

The choice of the location of the inflow plane was dictated by two considerations. First, a separate two-dimensional URANS computation for a cylinder was performed and compared to direct numerical simulation solutions by Tessicini et al.[25] for a Reynolds number of 3.9×10^3. (The value pertaining to the actual moving bar is 1.5×10^3.) This comparison showed that the wake statistics agreed reasonably well only within a streamwise distance of four diameters from the cylinder (Fig. 3). The secondary velocity defect seen at $x/D = 3$ in the simulation is due to a problem of stretched meshes around this particular position and is fully explained by Tessicini et al.[25] The location $0.32C$ upstream of the leading edge corresponds to three diameters downstream of the bar. Second, it is important to choose the inflow plane such that potential effects emanating from the inviscid flow/blade interaction are insignificant. This is the case at the chosen plane, as verified from the full blade/bar calculation.

The dissipation rate at the inflow boundary was then estimated from the mixing-length relationship

$$\varepsilon_{\text{in}} = c_\mu^{\frac{3}{4}} \left(k^{\frac{3}{2}} / l_{\text{mix}} \right) \tag{18}$$

where $l_{\text{mix}} = \alpha\delta$ is the mixing length for a wake, α is equal to 0.18 (Wilcox[26]), and δ is the half-width of the wake.

Figures 4a and 4b show the velocity and turbulence-energy profiles of the wake before it enters the blade passage at $x/C = -0.05$. Both velocity and turbulence-energy profiles are seen to correspond fairly well to the respective experimental profiles for the particular configuration examined.

IV. Results

A. Wake Characteristics

It is evident, from experiments as well as simulations, that the correct representation of the wake, in terms of the velocity perturbation it induces and the turbulence it transports, is the critical requirement in efforts to predict the average effects of the wake on the passage flow. Schulte and Hodson[20] show that the periodic passing of wakes reduces or eliminates the separation bubble observed in steady conditions on the suction side of the blade, with consequent reduction in profile losses. This effect is due to a combination of the inviscid,

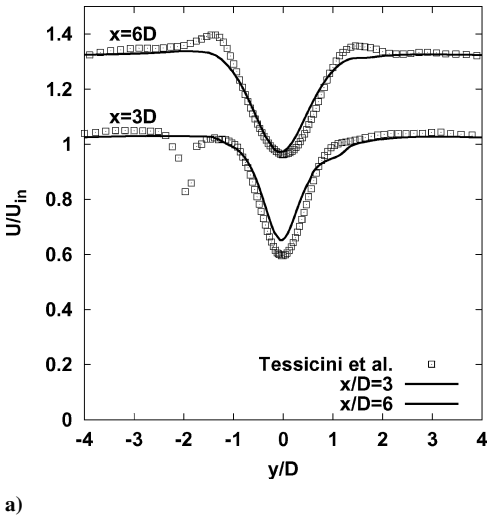

a)

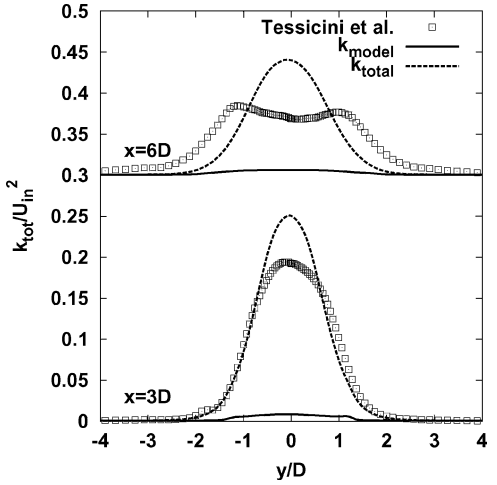

b)

Fig. 3 Flow around a circular cylinder at $Re_D = 3.9 \times 10^3$: a) velocity profiles and b) turbulence-energy profiles.

unsteady perturbations in the boundary layer, induced by the momentum defect of the wake, and the response of the boundary layer, in terms of its turbulence state, to the turbulence transported by the wake toward the boundary layer.

Although turbulence is generated in the shear layers of the wake, as well as by straining within the passage, convection of turbulence from the wake-generating device, especially within the passage, plays an important role with respect to both the aerodynamics of the wake and the response of the boundary layer to the wake turbulence. It follows, therefore, that the accuracy with which any inertial scalar quantity is transported within the passage is critically important. Thus, as a precursor to a discussion of results that depict the wake structure and its effects, Fig. 5 shows a numerical experiment in which a thin stream of an inert scalar quantity is being moved along the flow-inlet boundary, mimicking the moving wake, and convected through the passage, with physical diffusion removed.[24] The outcome of such a test should be a sharply delineated, deforming scalar wake, within which the value of the convected quantity is invariant and equal to the inlet level. As seen, this ideal is not reached even with the very fine grid and small time step adopted, but the quality of the solution is judged to be sufficient, the test conditions being considerably more demanding than in the actual wake/blade-interaction process.

An overall view of the manner in which the wake evolves in the passage and how it interacts with the boundary layer on the suction side is given in Figs. 6 and 7, which compare predicted with experimental turbulence-energy contours at eight phase (time) levels. Experimental results have been obtained by the use of

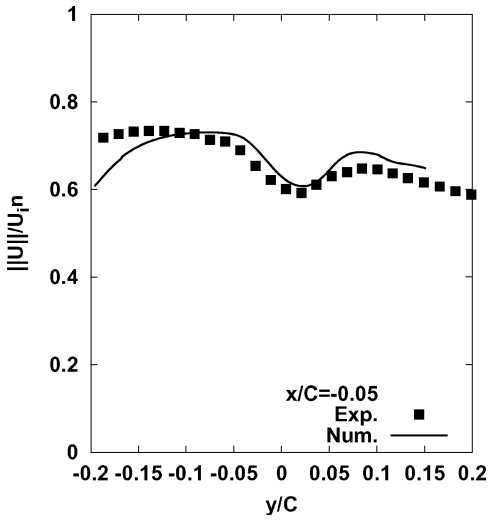

Fig. 4a Velocity profiles at a distance $x/C = -0.05$ from the leading edge of the blade.

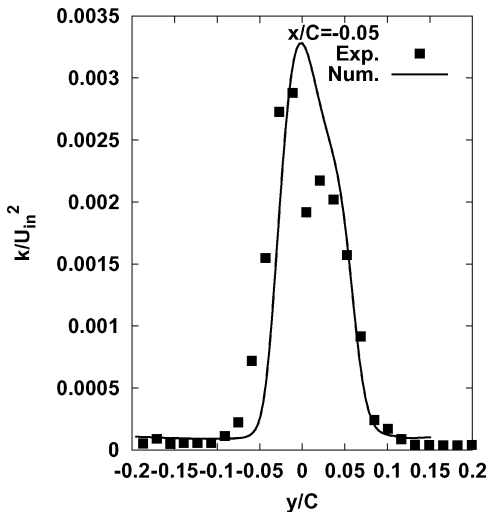

Fig. 4b Turbulence-energy profiles at a distance $x/C = -0.05$ from the leading edge of the blade.

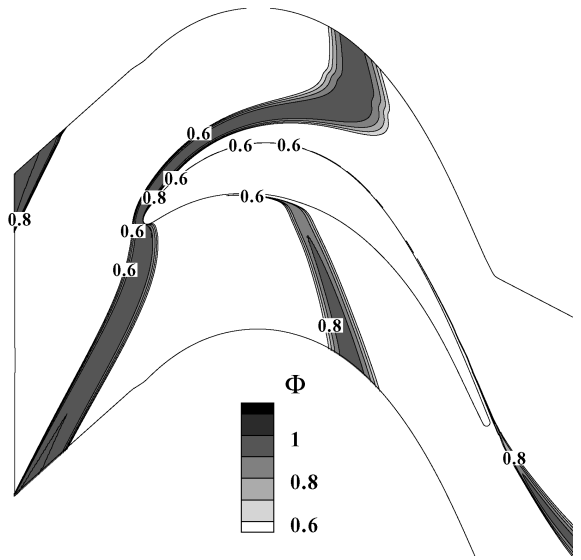

Fig. 5 Evolution of a passive-scalar stream of value 1 moved along the upstream boundary (151,000 grid cells, 800 time steps per traverse).

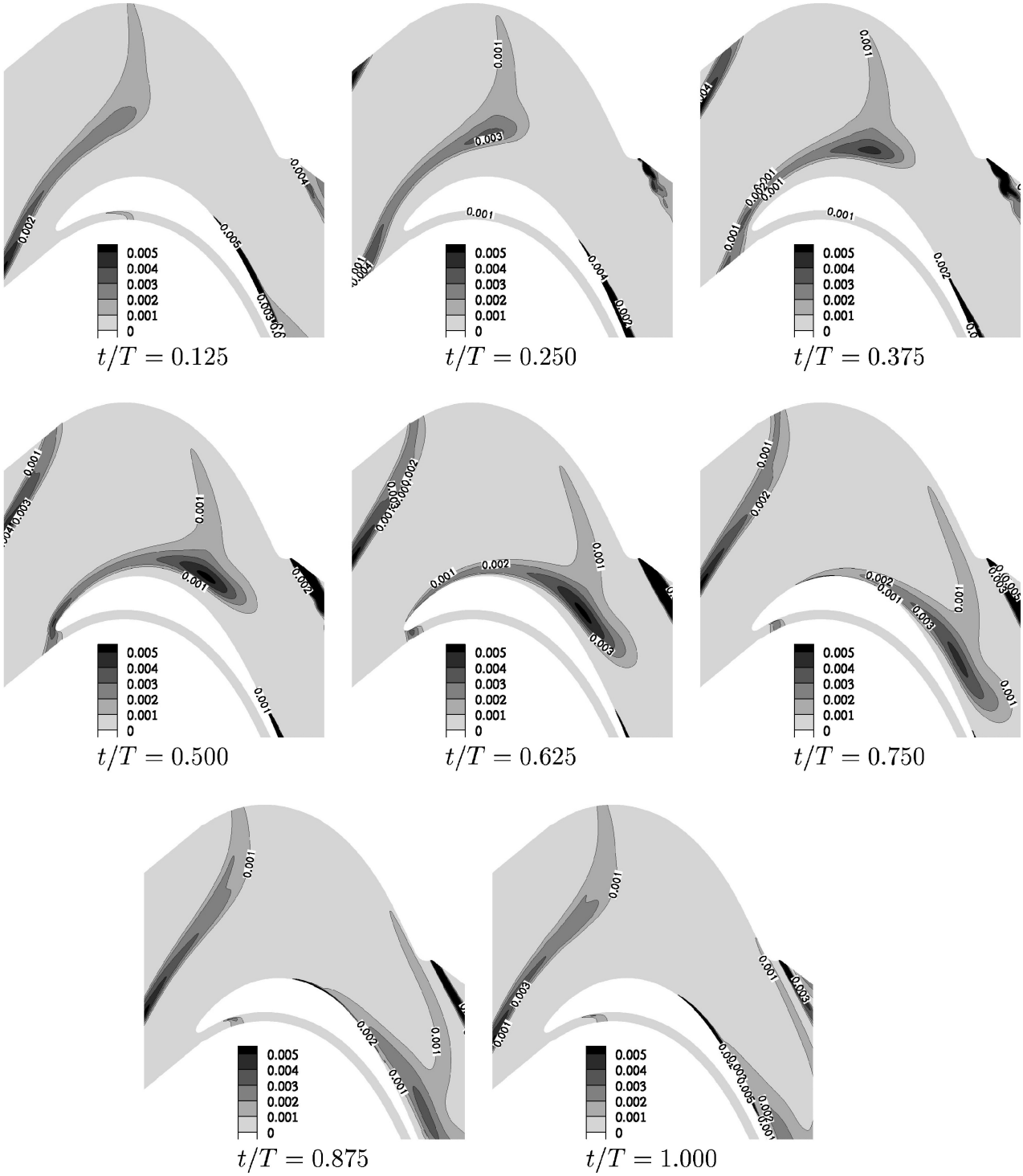

Fig. 6 Predicted isocontours of the turbulence energy k at eight different time levels.

two-dimensional laser Doppler anemometry (LDA) in combination with an ensemble-averaging technique that allowed converged phase-averaged data to be obtained.[15]

There are, evidently, remarkable qualitative similarities between the two sets of contours, and there is also a fairly close quantitative agreement in several respects. The computed wake is somewhat narrower than the experimental one, and this reflects mainly the thicker low-turbulence edges of the latter, as is also indicated in Fig. 4. At the same time, the computed peak turbulence levels are somewhat higher than those measured, typically by 20–30%. On the assumption that the experimental data are accurate, a possible origin of the differences is the limited ability of the URANS formulation to capture the dynamics associated with the large-scale structures emanating from the vigorous shedding behind the rods in the experimental configuration. Such structures would tend to enhance mixing and, hence, the spread of the wake to a larger extent than is captured by any RANS model. As expected, the computation resolves the vortex-shedding process at the rounded trailing edge, but it is important to point out, again, that the resolution of this feature, within a URANS methodology targeted toward a phase-averaged representation, is not really advantageous, for reasons discussed earlier in relation to the shedding behind the circular bars.

In both the computation and the experiment, the straining within the passage causes a significant increase in the turbulence energy in the wake. This is brought out well in Fig. 8, which shows contours of turbulence-energy production at the same eight time levels as

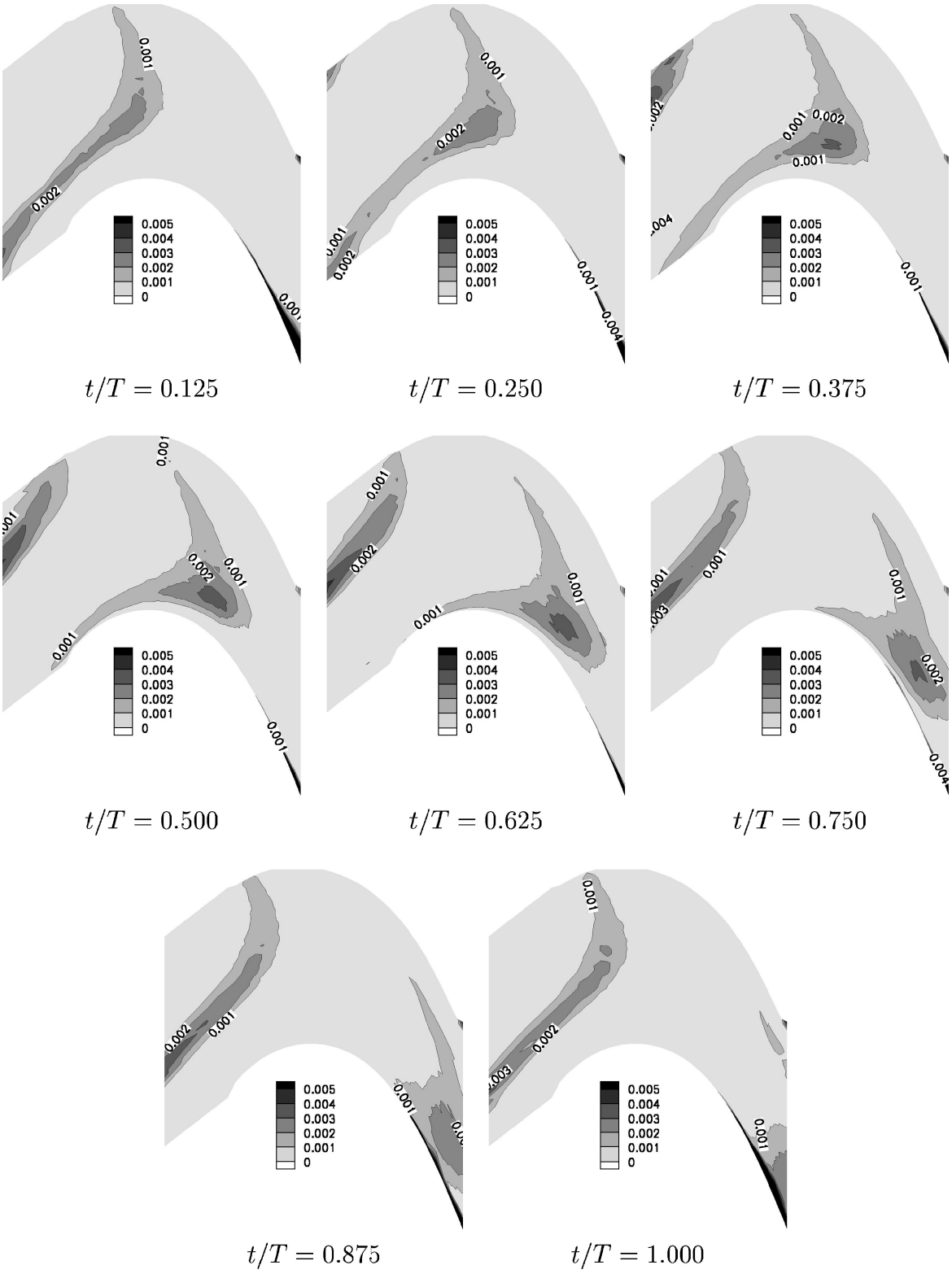

Fig. 7 Experimental isocontours of the turbulence energy k at eight different time levels.[15]

those in Figs. 6 and 7. As seen, production is especially high as the wake passes the region around 50% of the chord where the straining is highest. Toward the end of the traverse, when the wake exits the passage, the computed and experimental peak turbulence-energy levels are close to each other, and it is especially gratifying to observe that the wake-turbulence level is sustained at a broadly correct level right up to the end of the traverse, albeit at the penalty of the high computational cost associated with the fine grid and small time increment of the calculation.

Figure 6 also allows an initial view of the transitional response of the boundary layer to the wake; a discussion of quantitative details follows later. The boundary layer is predicted to be laminar across more than 70% of the suction side over most of the pitchwise traverse. At $t/T = 0.75$, a small patch of wake-induced turbulence in the boundary layer is observed at around $s/s_{\max} = 0.2 - 0.3$, with laminar flow persisting right up to the trailing edge. As the wake progresses, the patch grows and moves downstream. At $t/T = 1$, the boundary layer is turbulent over the rear 60% of the suction side.

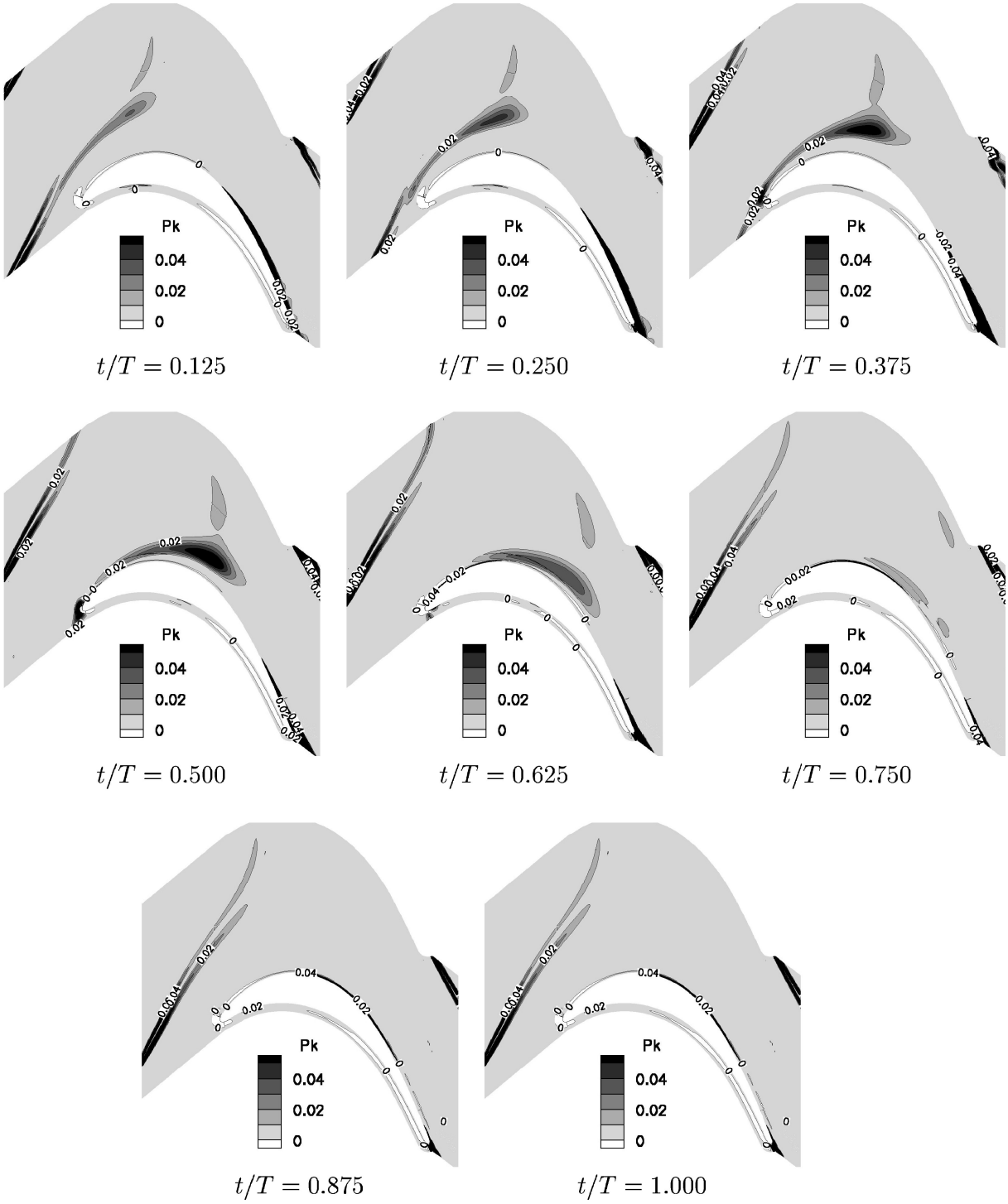

Fig. 8 Isocontours of the turbulence-energy production P_k at eight different time levels.

With the wake swept out of the domain and the time progressing from $t/T = 1$ to $t/T = 0.5$ (of the next traverse), turbulence in the boundary layer decays progressively, and the turbulent portion moves toward the rear of the suction side. Although difficult to see from the plots in Fig. 6 depicting the experimental turbulence-energy contours, a qualitatively similar behavior is observed in reality, although transition seems to occur further downstream, and the unsteadiness of the transitional process is lower. However, the measurements have been obtained by LDA, and so no data are available in the near-wall surface for the plots in Fig. 6. This will be dealt with hereafter.

As noted earlier, there is a view that the transition process is induced by dynamic disturbances associated with the wake's momentum deficit, whereas the wake's turbulence might only play a secondary role. The dynamic effects are brought to light in Fig. 9, which shows vector plots of the velocity perturbations, i.e., the difference between the phase-averaged velocity and the time-mean velocity. The wake is seen to induce two major rotational features on either side of the wake, denoted by D and E. The portion between features D and E is characterized by a pronounced (relative) downward motion toward the blade, often referred to as a *negative jet*. This "impinges" on the blade, causing a deceleration upstream of the jet and an acceleration downstream of it. Although not demonstrated herein, the computed perturbations have been found to be in good agreement with the experimental results of Stieger and Hodson.[6]

Schulte and Hodson[20] argue that the dynamic perturbation of the boundary layer provoked by this jet impingement, especially the deceleration and local separation, is the major ingredient in the process of wake-induced transition. Inspection of the velocity perturbation

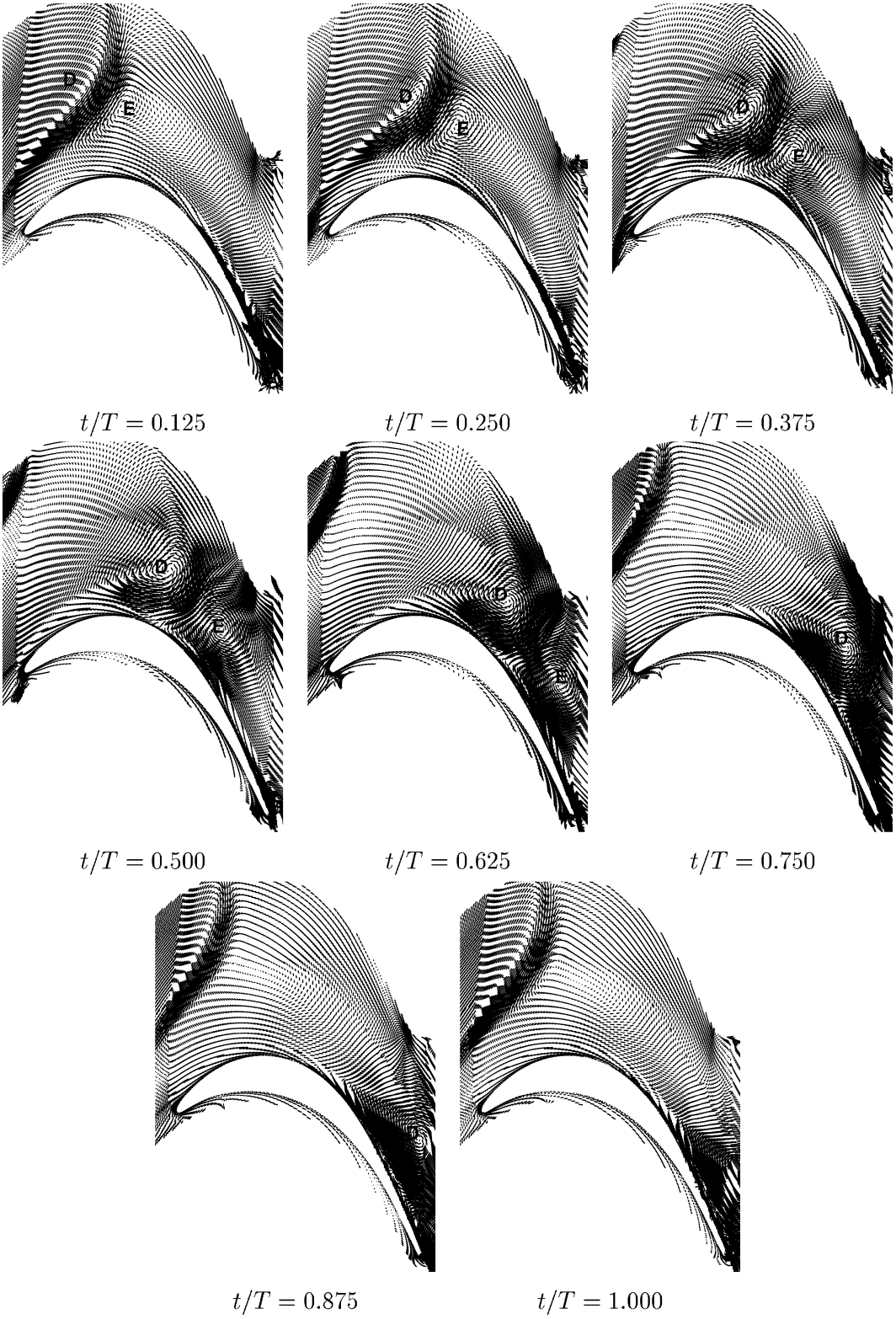

Fig. 9 Velocity perturbation vector fields at eight different time levels.

field in Fig. 9 reveals that the negative jet becomes an established feature over the suction side at around $t/T = 0.375$. Over the period $0.375 < t/T < 1$, the impingement point moves toward the trailing edge, from $s/s_{\max} = 0.3$ to about $s/s_{\max} = 0.9$. Figure 6 shows, however, that transition in the suction-side boundary layer at $t/T = 0.75$ and 0.875 begins well upstream of the negative jet, namely, when the wake turbulence reaches the boundary layer. Hence, the URANS computation appears to suggest that the boundary layer is at least receptive to wake turbulence as the latter reaches the edge of the boundary layer. The deceleration associated with the negative jet may be an influential feature, but is not predicted to be the principal, and certainly not the only, feature responsible for transition.

In an effort to convey a clearer view on the dependence of transition on the dynamics and turbulence of the wake, Figs. 10 and 11 give, respectively, the absolute-velocity and velocity-perturbation plots immediately above the suction side in the trailing-edge region $0.9 < s/s_{\max} < 1$. Superimposed are contours of turbulence energy. Note that the upper end of the energy scale is much higher than that

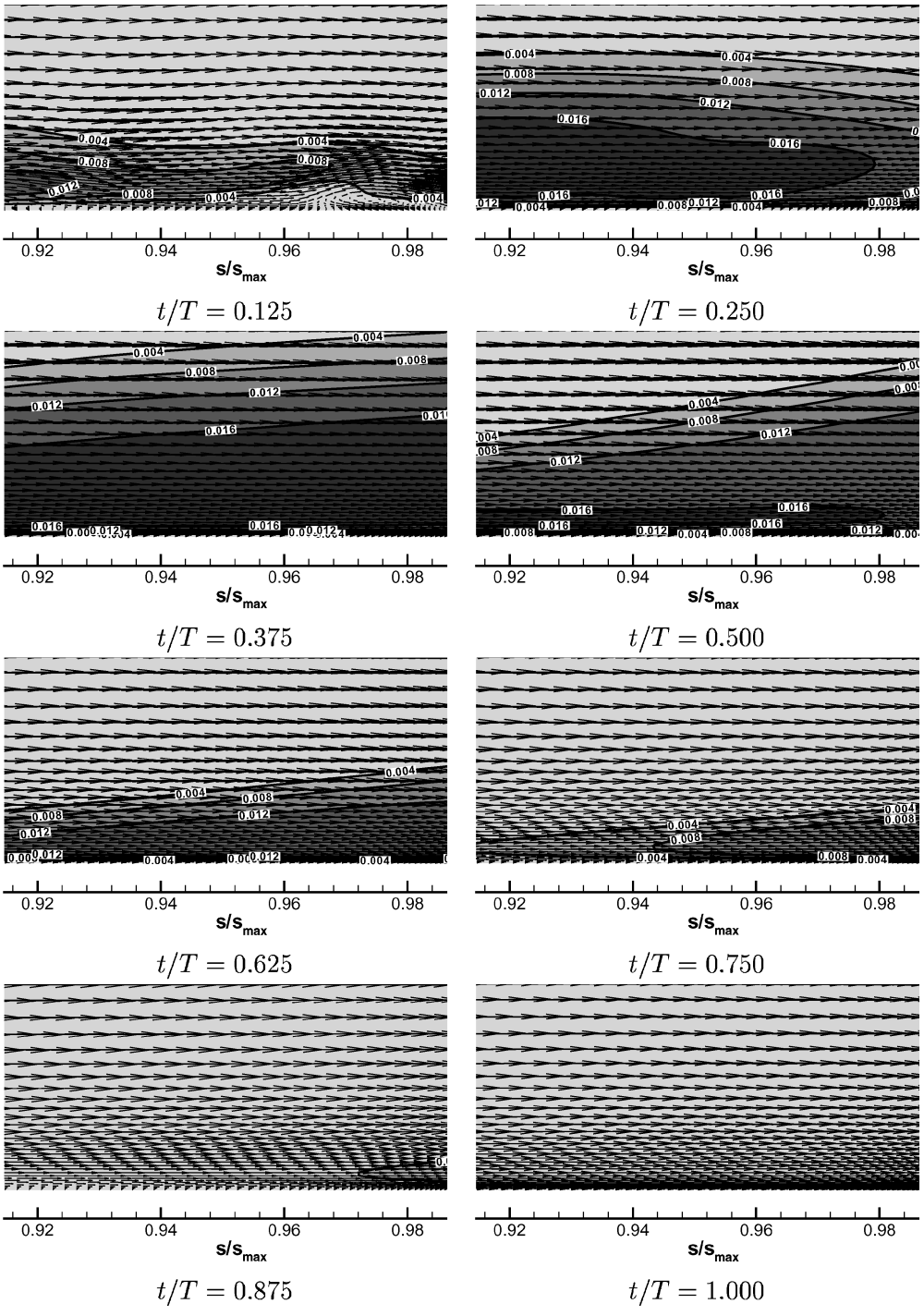

Fig. 10 Turbulence energy k and velocity vectors near the trailing edge of the blade at eight different time levels.

in Fig. 6, to accommodate the high levels encountered in the turbulent boundary layers. Figure 10 shows that the boundary layer is separated or is close to separation from $t/T = 0.875$ to $t/T = 0.25$. This is closely associated with strong reverse relative motion just above the blade surface (Fig. 11) and is related to the negative jet. However, at $t/T = 0.875$ and 1, the boundary layer on the rear-most portion of the suction side is not turbulent, and there is no indication of transition being initiated at that stage. Rather, turbulence in this region arises later, beyond $t/T = 0.125$, and this appears to be associated with the turbulence tail of the previous wake, which is clearly seen in the plot of the turbulence-energy contours at $t/T = 0.125$, Fig. 6. These observations strengthen our conclusion that transition is induced, in the URANS computation, principally by wake turbulence, rather than by the dynamic wake effects. However, it is not really possible to separate, unambiguously, the effect of the perturbations from that of wake turbulence on the transition process because transition is predicted to start not much later after the dynamic effects provoke reverse flow in the boundary layer. This separation is made all the more difficult by the fact that the turbulence intensity rises in the region of the negative jet due to the increased strain adding to the turbulence generation.

B. Space/Time Plot

The transitional response of the boundary layer to the passing wakes is well conveyed by plots of integral boundary-layer quantities in a time/space domain, with the abscissa covering the leading-to-trailing-edge distance along the suction side and the ordinate the pitchwise phase (or time) passage. Figure 12 compares predicted and experimental shape-factor variations. Two predicted fields are included, one with a model version that respects the wall-asymptotic

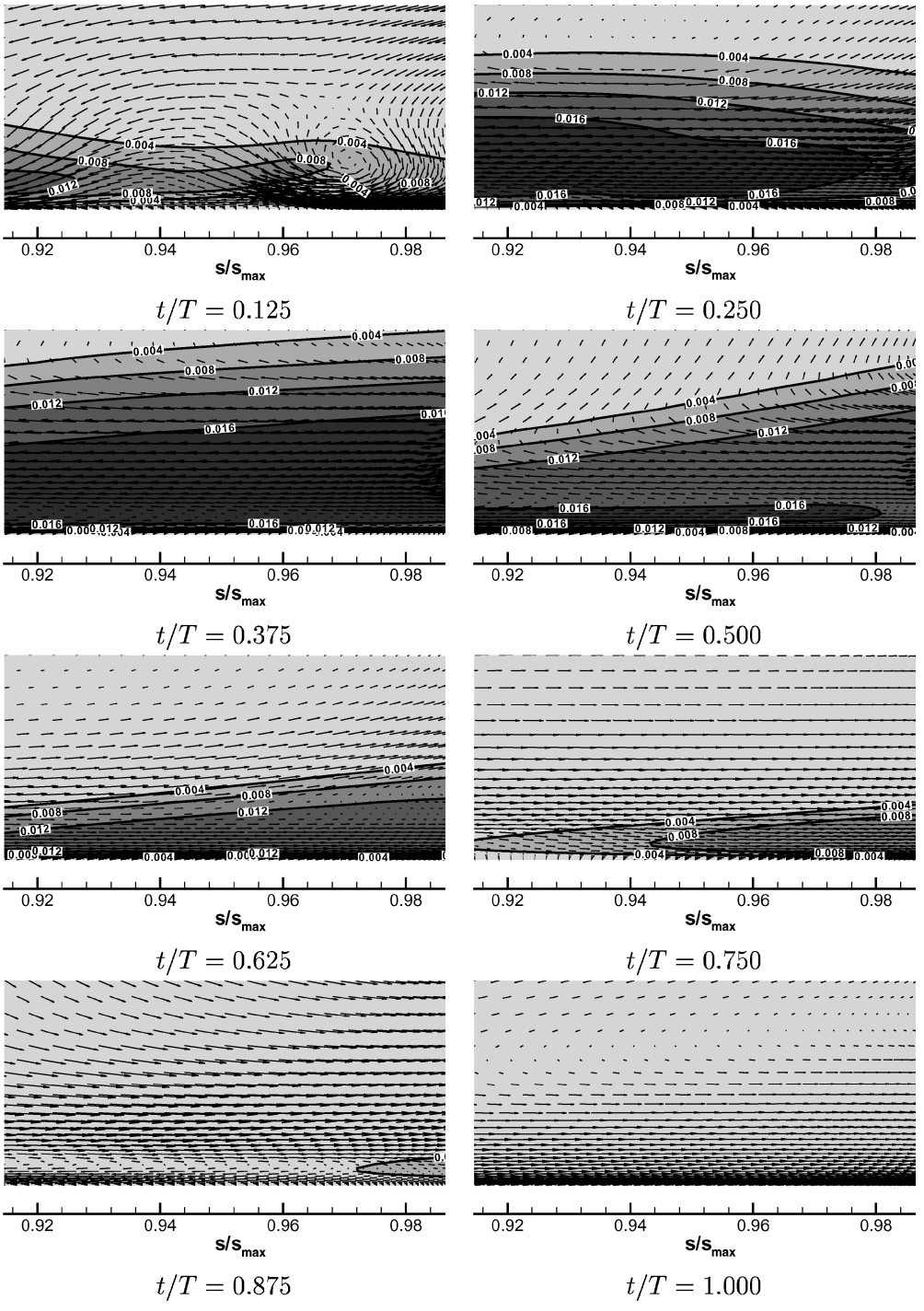

Fig. 11 Turbulence-energy k and perturbation velocity vector fields near the trailing edge of the blade at eight different time levels.

variation of turbulence anisotropy [Eq. (8)] and the other [Eq. (9)] that ignores the influence of the wall-distance dependence of the model. Following Stieger's[15] notation, lines are included on the plots in Fig. 12 to identify specific regions. Line A indicates the region where the velocity reaches a maximum at the upper edge of the boundary layer, and line B marks the minimum velocity, which occurs after the negative jet has passed. Experimental data are only available beyond $s/s_{\max} = 0.5$. These imply that boundary-layer transition occurs at around $s/s_{\max} = 0.7$, that the boundary layer is always turbulent and attached beyond $s/s_{\max} = 0.9$, and that a separated state exists in the region $s/s_{\max} = 0.6 - 0.9$ over about 60% of the pitchwise period. As seen, there are some strong qualitative similarities between the computations and the experiment, especially that with model 1 [Eq. (8)]. In both, the wake path is clearly visible. As in the experiment, the computation shows that the rear portion of the suction side is characterized by alternate periods of attached/turbulent and separated/laminar flow. The computed increase in H upstream of $s/s_{\max} = 0.6$ along the wake indicates spots of increased boundary-layer thickness resulting from the passage of the wake-turbulence cloud. There is no real transition in this part because H remains around 2.25, but there is an effect of the wake on the boundary layer, which reverses, however, as the wake progresses. High levels of turbulence are only provoked beyond $s/s_{\max} = 0.6$. A double peak identified in Fig. 12 by C and D, appearing at around $s/s_{\max} = 0.7$ and observed experimentally by Stieger and Hodson,[6] is correctly predicted in both computations. These two structures are attributed by Stieger and Hodson to the interaction between the wake and the detached boundary layer. A point of difference relates to the state of the boundary layer over the last 10% of the suction side, insofar as the computation predicts a

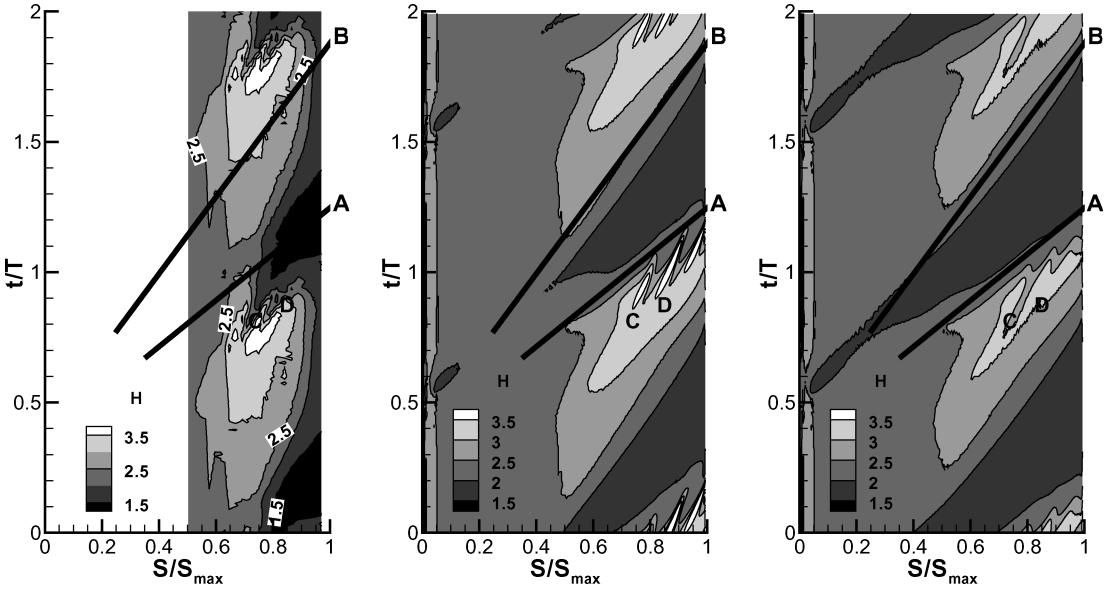

a) Experiment[15] b) Abe et al.[18] model 1, Eq. (8) c) Abe et al.[18] model 2, Eq. (9)

Fig. 12 Space/time plots of the shape factor H.

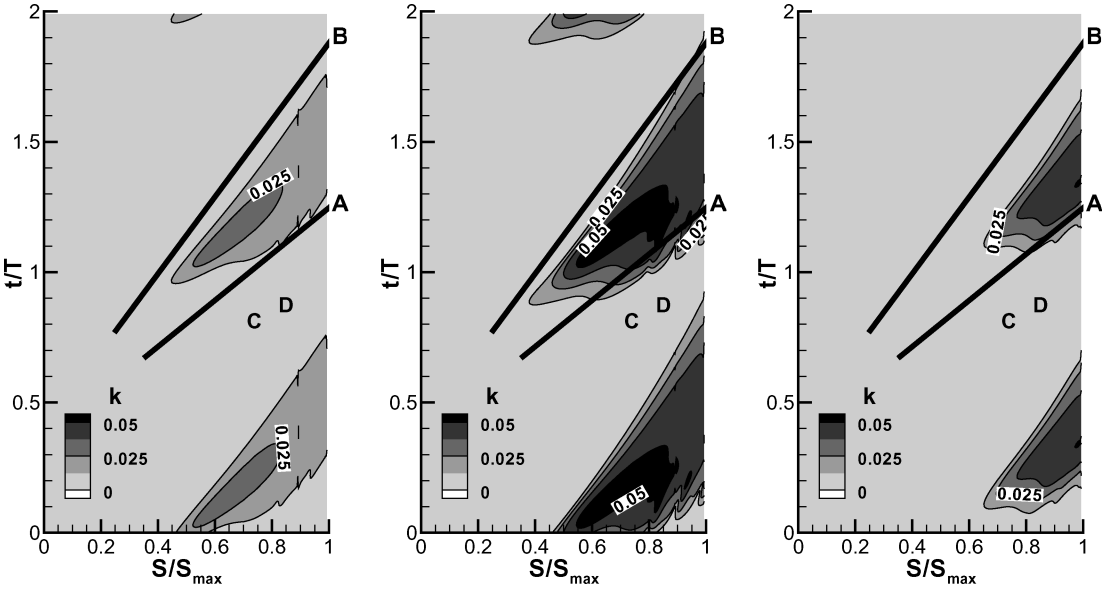

a) $y/c = 0.00068$ b) $y/c = 0.0034$ c) $y/c = 0.01374$

Fig. 13 Space/time plots of the turbulence-energy k at three different distances from the wall, Abe et al.[18] model 1 [Eq. (8)].

laminar, separated flow over about $0.2T$, whereas the experiments suggest that the boundary layer in that region is fully attached and turbulent. A possible explanation for this discrepancy stems from the fact that, for this configuration, the freestream-turbulence intensity is very low (below 1%), and that the model fails to predict a correct natural transition. This defect has already been addressed by Lardeau et al.,[11] and it has been observed that this defect is accentuated by an adverse pressure gradient, as is present in the trailing-edge region of the blade. Importantly, however, the computation captures the strong reduction of separation due to the wake and the calming phenomenon. The comparison between the computations with the two model versions leads to the conclusion that refined modeling of the near-wall region can be influential and beneficial.

Figure 13 finally shows contours of turbulence energy across three planes parallel to the suction side at three different distances from the wall. Very close to the wall, as well as close to the edge of the boundary layer, turbulence is low, whereas in the central portion of the boundary layer, turbulence is high. The middle and rightmost plots in Fig. 13 both reveal the path of the wake cloud and suggest further that turbulence is induced by this cloud and amplified within the boundary layer, starting at around $s/s_{\max} = 0.6$.

V. Conclusions

A number of issues pertaining to the prediction of wake/blade interaction with an unsteady RANS approach have been investigated. Three major aspects have been considered, in particular, 1) the level of spatial and time resolution required to attain sufficient numerical accuracy, 2) the best approach to the generation of the wake and its introduction into the blade domain, and 3) the ability of the particular low-Reynolds-number turbulence model to represent the effects of the wake on the transitional characteristics of the blade boundary layer, among them the periodic separation and reattachement induced by the passing wakes.

In terms of numerical resolution, it has been demonstrated that, notwithstanding the use of higher-order discretisation, a very fine grid and a very small time step are needed for numerical contamination to be reduced to a sufficiently low level.[24] This is due to the dominance of convective transport as the wake progresses across

the blade passage, the fact that the motion of the wake is not aligned with the grid lines, and the need to resolve to a high level of accuracy the scalar turbulence fields associated with the wake in which turbulence is far from a state of equilibrium.

As to the generation of the wake, the natural approach of including the bar and the flow around it within the URANS computation was shown to be fraught with problems and was, thus, judged to be inappropriate. The main problem is that the bar generates a von Kármán vortex street, the behavior of which is badly represented, even in statistical terms, with a two-dimensional URANS method beyond about four bar diameters. In part, this is due to the organized unsteady motion associated with the shed vortices decaying too slowly, the absence of a mechanism for spanwise breakdown, and the modeled turbulence energy being much too low. Also, the small timescale associated with the shedding is inappropriate within a phase-averaged RANS approach, which is oriented toward the timescale of the pitchwise-traverse period. This then led to a methodology in which a precomputed wake, appropriately averaged, was prescribed downstream of the bar. The need to do so and the underlying reasons clearly have some serious implications for practical URANS computations of rotor/stator interaction problems.

With the wake prescribed, as indicated, the particular low-Reynolds-number nonlinear eddy-viscosity model adopted has been shown to perform well in predicting the principal unsteady transitional features of the suction-side boundary layer, including the unsteady separation and reattachment provoked by the wakes. The becalmed region observed between the passing wakes is also well reproduced. The computations suggest that the wake-induced transition is mainly due to the diffusion of the turbulence energy transported by the wake into or toward the edge of the boundary layer, rather than a result of dynamic processes induced in the boundary layer by the momentum deficit of the wake, as assumed by Stieger and Hodson.[6] Nevertheless, the overall effect is the same, namely, the suppression of the separation bubble observed in steady cases.

Despite a good overall agreement between the computation and the experiment, several quantitative discrepancies have been observed. First, the predicted production of turbulence energy in the downstream part of the passage is higher than in the experiment. Second, due to the very low level of freestream turbulence between the wakes, the model is not able to predict the natural transition observed experimentally between the passing wakes in the rear-most part of the blade. This defect is also observed in steady conditions; for example, in flow over a flat plate at low freestream turbulence. However, in realistic turbine operation, the level of turbulence is much higher, and this can be expected to favor the performance of the present model. To substantiate this assumption, further experiments at higher turbulence intensity are needed.

Acknowledgment

The research reported in this paper was undertaken within the project "Unsteady Transitional Flows in Axial Turbomachinery," funded by the European Commission under Contract G4RD-CT-2001-00628.

References

[1]Wu, X., Jacobs, R. G., Hunt, J. C. R., and Durbin, P. A., "Simulation of Boundary Layer Transition Induced by Periodically Passing Wakes," *Journal of Fluid Mechanics*, Vol. 398, 1999, pp. 109–153.

[2]Michelassi, V., Wissink, J. G., Frölich, J., and Rodi, W., "Large-Eddy Simulation of Flow Around Low-Pressure Turbine Blade with Incoming Wakes," *AIAA Journal*, Vol. 41, No. 11, 2003, pp. 2143–2156.

[3]Wissink, J. G., "DNS of Separating, Low Reynolds Number Flow in a Turbine Cascade with Incoming Wakes," 5th International Symposium on Engineering Turbulence Modelling and Measurements, Sept. 2002.

[4]Mayle, R. E., "The Role of Laminar–Turbulent Transition in Gas Turbine Engines," *Journal of Turbomachinery*, 1991, Vol. 113, pp. 509–537.

[5]Stieger, R. D., and Hodson, H. P., "Unsteady Surface Pressures Due to Wake Induced Transition in a Laminar Separation Bubble on a LP Turbine Cascade," American Society of Mechanical Engineers, ASME Turbo Expo, Power for Land, Sea and Air, Paper GT2003-38303, June 2003.

[6]Stieger, R. D., and Hodson, H. P., "The Transition Mechanism of Highly-Loaded LP Turbine Blades," American Society of Mechanical Engineers, ASME Turbo Expo, Power for Land, Sea and Air, Paper GT2003-38304, June 2003.

[7]Savill, A. M., *By-Pass Transition Using Conventional Closures*, edited by B. Launder and N. Sandham, Cambridge Univ. Press, Cambridge, England, U.K., 2001, pp. 464–492.

[8]Chen, W. L., Lien, F. S., and Leschziner, M. A., "Non-Linear Eddy-Viscosity Modelling of Transitional Boundary Layers Pertinent to Turbomachine Aerodynamics," *International Journal of Heat and Fluid Flow*, Vol. 19, 1998, pp. 297–306.

[9]Steelant, J., and Dick, E., "Modelling of Laminar-Turbulent Transition for High Freestream Turbulence," *Journal of Fluids Engineering*, Vol. 123, 2001, pp. 22–30.

[10]Suzen, Y. B., and Huang, P. G., "Modelling of Flow Transition Using an Intermittency Transport Equation," *Journal of Fluids Engineering*, Vol. 122, 2000, pp. 273–284.

[11]Lardeau, S., Leschziner, M.A., and Li, N., "Modelling Bypass Transition with Low-Reynolds-Number Non-Linear Eddy-Viscosity Closure," *Flow, Turbulence and Combustion* (to be published).

[12]Lübcke, H., Schmidt, St., Rung, T., and Thiele, F., "Comparison of LES and RANS in Bluff-Body Flows," *Journal of Wind Engineering and Industrial Aerodynamics*, Vol. 89, 2001, pp. 1471–1485.

[13]Rodi, W., *Large-Eddy Simulation of the Flow Past Bluff Bodies*, Cambridge Univ. Press, Cambridge, England, U.K., 2002, pp. 361–391.

[14]Yao, Y. F., Savill, A. M., Sandham, N. D., and Dawes, W. N., "Simulation and Modelling of Turbulent Trailing-Edge Flow," *Flow, Turbulence and Combustion*, Vol. 68, 2002, pp. 313–333.

[15]Stieger, R. D., The Effects of Wakes on Separating Boundary Layers in Low-Pressure Turbines, Ph.D. Dissertation, Engineering Dept. Cambridge Univ., Cambridge, England, U.K., Feb. 2002.

[16]Wu, X., and Durbin, P. A., "Evidence of Longitudinal Vortices Evolved from Distorted Wakes in a Turbine Passage," *Journal of Fluid Mechanics*, Vol. 446, 2001, pp. 199–228.

[17]Catalano, P., Wang, M., Iaccarino, G., and Moin, P., "Numerical Simulation of the Flow Around a Circular Cylinder at High Reynolds Number," *Engineering Turbulence Modelling and Experiment*, 5th International Symposium on Engineering Turbulence Modelling and Measurements, edited by W. Rodi and N. Fueyo, Mallorca, Spain, 2003.

[18]Abe, K., Jang, Y.-J., and Leschziner, M. A., "An Investigation of Wall-Anisotropy Expressions and Length-Scale for Non-Linear Eddy-Viscosity Models," *International Journal of Heat and Fluid Flow*, Vol. 28, No. 2, 2002, pp. 181–198.

[19]Wang, C., Jang, Y.-J., and Leschziner, M. A. "Modelling 2D and 3D Separation from Curved Surfaces with Anisotropy-Resolving Turbulence Closures," *Procedings of the 3rd International Symposium on Turbulence and Shear Flow Phenomena*, Sendai, Japan, 2003.

[20]Schulte, V., and Hodson, H. P., "Unsteady Wake-Induced Boundary Layer Transition in High-Lift LP Turbine, American Society of Mechanical Engineers, ASME Paper 96-GT-486, 1996.

[21]Lien, F. S., Chen, W. L., and Leschziner, M. A., "A Multiblock Implementation of a Non-Orthogonal Collocated Finite Volume Algorithm for Complex Turbulent Flows," *International Journal of Numerical Methods in Fluids*, Vol. 23, 1996, pp. 567–588.

[22]Chen, W. L., and Leschziner, M. A., "Turbulence Modelling of Rotor–Stator Interaction with Linear and Non-Linear Eddy-Viscosity Models," *3rd European Conference on Turbomachinery*, Vol. A, Paper C557/130/99, IMechE, London, 1999.

[23]Lien, F. S., and Leschziner, M. A., "A General Non-Orthogonal Collocated Finite Volume Algorithm for Turbulent Flow at All Speeds Incorporating Second-Moment Turbulence-Transport Closure, Part 1: Computational Implementation," *Computer Methods in Applied Mechanics and Engineering*, Vol. 114, 1994, pp. 123–148.

[24]Lardeau, S., and Leschziner, M. A., "Unsteady RANS Simulation of Wake–Blade Interaction: Computational Requirements and Limitations," *Computers and Fluids* (to be published).

[25]Tessicini, F., Leonardi, S., and Orlandi, P., "DNS&LES of Complex Flows Using an Immersed Boundary Method," Fifth World Congress on Computational Mechanics, Vienna, July 2002.

[26]Wilcox, D. C., *Turbulence Modelling for CFD*, DCW Industries, La Canada, CA, 1998, pp. 32–38.

R. So
Associate Editor